Iranian Society of Acoustics and Vibration
The 14th ISAV2024 International Conference on Acoustics and Vibration
11-12 Dec 2024 Karaj - Iran
Kharazmi University

On the Oscillatory Behavior of Silver and Gold Nanoparticles Inside Lipid Nanotubes

Fatemeh Sadeghi[a*]

[a] *Associate Professor, Department of Engineering Sciences, Faculty of Advanced Technologies, University of Mohaghegh Ardabili, 56318-44133, Namin, Iran.*

** Corresponding author e-mail: f.sadeghi@uma.ac.ir*

Abstract

This research investigates the oscillatory behavior of metallic nanoparticles, specifically silver and gold nanoparticles, inside lipid nanotubes (LNTs) utilizing the continuum approximation and the 6-12 Lennard-Jones (LJ) potential function. The nanoparticle is represented as a dense sphere, and the LNT is considered to have six layers: two head groups, two intermediate layers, and two tail groups. In order to determine the van der Waals (vdW) interactions between the two interacting nanostructures, analytical expressions are derived by undertaking surface and volume integrals. Ignoring the frictional forces and utilizing the Runge-Kutta numerical integration scheme, the equation of motion is directly solved to attain the time histories of displacement and velocity of silver and gold nanoparticles inside LNTs. Based on the conservation of mechanical energy principle, a new oscillation frequency formula is also derived to precisely evaluate the frequencies of the proposed nano-oscillator. The effects of initial conditions and geometrical parameters on the oscillatory behavior of system are examined. Numerical results indicate that silver nanoparticle generates higher frequencies inside LNTs compared to gold nanoparticle. It is further found that the tail group thickness has a smaller effect on the oscillation frequency than the head group thickness.

Keywords: Metallic nanoparticles; Lipid nanotubes; Continuum approximation; Oscillation frequency.

1. Introduction

Metallic nanoparticles have been the focus of attention for more than a century due to their superior optical, electrical, and thermal capabilities [1,2]. Silver and gold nanoparticles, created either intra-or extra-cellularly using living organisms, are extremely valuable. These materials have a wide range of applications in science and technology, including drug delivery, probes for electron microscopy to visualize cellular components, diagnosis and therapy, textile coatings, electronics,

biosensors, and so on [3-5]. Lipid nanotubes (LNTs) are also thought to be among of the biggest examples of self-organized nonliving structures that have been discovered to date [6]. Many applications in material science, chemistry, biochemistry, medicine, and as templates for structured nanomaterials are made possible by the unique advantages of LNTs over other materials [7]. These properties include high biocompatibility, controllability of diameters, lengths, and wall thickness, less vulnerability to microbial attack, large inner volumes, accessibility to inner surfaces, and capacity to functionalize outer surfaces [8].

LNTs are open-ended, hollow cylindrical structures made of rolled-up lipid bilayer membrane walls. The lipid bilayer, also known as the phospholipid bilayer, is extremely thin in comparison to its lateral dimensions [9]. Although the thickness of a lipid bilayer is a few nanometers, it is comprised of several distinct chemical regions across its cross-section. The fully hydrated hydrophilic head group is the initial region on either side of the bilayer, measuring around 0.8-0.9 nm thick. The second region is the intermediate layer, which is adjacent to the hydrated region and is slightly hydrated with a thickness of around 0.3 nm. The hydrophobic core of the bilayer is also completely dehydrated with a thickness of 3-4 nm. In addition, the thickness of a lipid bilayer varies with chain length and chemistry [10], as well as with temperature, particularly near a phase transition [11].

In the published literature, the interactions between lipid bilayer and various nanostructures have been thoroughly investigated using both the molecular dynamics (MD) simulations and the continuum approximation. In this regard, Berger et al. [12] utilized the Lennard-Jones (LJ) potential function and an electrostatic term as the force field to perform an MD study on the interaction for the lipid bilayer of dipalmitoylphosphatidylcholine (DPPC), a phospholipid composed of two palmitic acids, under different conditions. Qiao et al. [13] examined the translocation of C_{60} fullerene and its derivative across a DPPC lipid bilayer. Based on the MD simulations, Wang et al. [14] reported that the interaction between membranes of DPPC lipids and single-walled carbon nanotubes is concentration-dependent. Other researchers used a coarse grain method [15] to simulate the complicated structure of the lipid bilayer. According to Shelley et al. [16], simulating the self-assembly of phospholipids using the coarse grain technique is more effective than using Monte Carlo simulations. Baowan et al. [17] conducted a study on the interactions between a C_{60} fullerene and a lipid bilayer using the coarse grain model and the continuum approximation. Similarly, Sukchom et al. [18] investigated the penetration of a carbon nanocylinder through a lipid bilayer on the same basis. Employing the continuum approximation along with the 6-12 LJ potential function, Sadeghi et al. [19] also studied the issues of suction energy and acceptance condition of metallic nanoparticles (silver and gold) inside LNTs. Their study revealed that the maximum suction energy decreases with increasing head group or tail group thickness, but increases with nanoparticle size.

Many scientists throughout the world have shown technical interest in ultrahigh-frequency nano-oscillators, whose frequencies are in the range of gigahertz (GHz) or beyond. These nano-oscillators have a variety of applications, including ultra-fast optical filters for fiber optic systems and nanoantennas sensitive to high-frequency electromagnetic signals. Furthermore, high-frequency nano-oscillators have been proposed for applications in ultra-sensitive detector devices, radio frequency signal processing, and as a model system for exploring quantum phenomena in macroscopic systems [20-22]. This study aims to present a continuum-based model to investigate the oscillatory behavior of silver and gold nanoparticles inside LNTs. Based on the continuum approximation along with the classical LJ potential function, analytical expressions are introduced to determine the vdW interactions between the two interacting molecules. Ignoring the frictional forces, the equation of motion is solved numerically to obtain the time histories of displacement and velocity of silver and gold nanoparticles inside LNTs. Employing the conservation of mechanical energy principle, a new frequency formula is also derived to evaluate the oscillation frequencies of nano-oscillator under different system parameters.

2. Potential energy and interaction force

Figure 1 shows a dense spherical nanoparticle of radius R_p located on the axis of a LNT of innermost radius R_l and length $2L$. The LNT has six layers: two head, two intermediate, and two tail groups. The intermediate layer is a cylindrical surface, whereas the head and tail groups are cylinders with thicknesses of H_h and H_t, respectively. According to Fig. 1, the six radii of LNT are defined by

$$\begin{aligned} &R_{l_1} = R_l, && R_{l_2} = R_{l_1} + H_h, && R_{l_3} = R_{l_2} + H_t, \\ &R_{l_4} = R_{l_3} + \delta, && R_{l_5} = R_{l_4} + H_t, && R_{l_6} = R_{l_5} + H_h \end{aligned} \tag{1}$$

in which $\delta = 3.36\,\text{Å}$ is the equilibrium gap between two layers of a lipid bilayer [17].
Thus, the total potential energy is obtained by summing the interactions between nanoparticle and the six layers of LNT as [19]

$$\begin{aligned} E^{(tot)}(Z) &= E_{pi}\left(Z, R_{l_2}, A_{pi}, B_{pi}\right) + E_{pi}\left(Z, R_{l_5}, A_{pi}, B_{pi}\right) \\ &+ E_{ph}\left(Z, R_{l_1}, R_{l_2}, A_{ph}, B_{ph}\right) + E_{ph}\left(Z, R_{l_5}, R_{l_6}, A_{ph}, B_{ph}\right) \\ &+ E_{pt}\left(Z, R_{l_2}, R_{l_3}, A_{pt}, B_{pt}\right) + E_{pt}\left(Z, R_{l_4}, R_{l_5}, A_{pt}, B_{pt}\right) \end{aligned} \tag{2}$$

where E_{pi} denotes the nanoparticle-intermediate interactions, while E_{ph}/E_{pt} denotes the nanoparticle-head/tail group interactions. Moreover, A_{pi}/B_{pi}, A_{ph}/B_{ph} and A_{pt}/B_{pt} are the attractive/repulsive constants between nanoparticle and intermediate layer, nanoparticle and head group and nanoparticle and tail group, respectively which are obtained through mixing rules [19]. Following [19], E_{pi} and E_{ph}/E_{pt} can be written as

$$E_{pi}\left(Z, R, A, B\right) = \Gamma_s \sum_{n=1}^{2} (-1)^{(n+1)} \left(G_1 \tan^{-1} \chi_n + \sum_{m=1}^{8} G_{2m-1} \frac{\chi_n}{\left(1+\chi_n^2\right)^m} \right) \tag{3}$$

$$E_{ph/pt}\left(Z, r_1, r_2, A, B\right) = \Gamma_v \sum_{n=1}^{2} \sum_{j=1}^{2} (-1)^{(n+1)} \left(G_{1j} \tan^{-1} \chi_{nj} + \sum_{m=1}^{7} G_{(2m-1)j} \frac{\chi_{nj}}{\left(1+\chi_{nj}^2\right)^m} \right) \tag{4}$$

where $\Gamma_s = 2\pi R_i \eta_i \gamma$, $\Gamma_v = \pi \eta_{h/t} \gamma$ and $\gamma = 4/3\,\pi R_p^3 \eta_p$; $\chi_n = Z_n/\lambda$, $\chi_{nj} = Z_n/\lambda_j$ and $Z_1 = Z + L$, $Z_2 = Z - L$, $\lambda = \sqrt{R_i^2 - R_p^2}$ and $\lambda_j = \sqrt{r_j^2 - R_p^2}$. Also, $G_1, G_{1j}, G_{2m-1}, G_{(2m-1)j}$ are defined in [19].
Furthermore, the total vdW force is obtained by differentiating the total potential energy as follows

$$F_{vdW}^{(tot)} = -\nabla E^{(tot)} \tag{5}$$

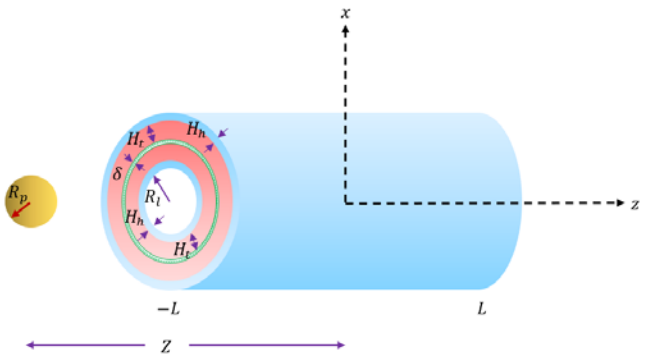

Figure 1. Geometry of metallic nanoparticle-LNT oscillators.

3. Equation of motion and the frequency of oscillation

Using the Newton's second law, the equation of motion is given by

$$m_p \ddot{Z}(t) = F_{vdW}^{(tot)}(Z) \tag{6}$$

in which m_p shows the mass of nanoparticle.

Solving Eq. (6) numerically yields the oscillation frequency. The oscillation frequency can be also obtained from the energy equation. Ignoring the frictional forces [23] and employing the conservation of mechanical energy law gives

$$\frac{1}{2}m_p\dot{Z}^2(t)+E^{(tot)}(Z)=E^{(tot)}(A_0)\rightarrow\sqrt{\frac{m_p}{2}}\int_0^{A_0}\frac{dZ}{\sqrt{E^{(tot)}(A_0)-E^{(tot)}(Z)}}=\int_0^{\frac{T}{4}}dt \tag{7}$$

where A_0 is the amplitude of motion and the period of motion can be calculated from

$$T=2\sqrt{2m_p}\int_0^{A_0}\frac{dZ}{\sqrt{E^{(tot)}(A_0)-E^{(tot)}(Z)}} \tag{8}$$

The period of motion can be obtained by summing T_1 and T_2 as

$$T_1=2\sqrt{2m_p}\int_0^{cA_0}\frac{dZ}{\sqrt{E^{(tot)}(A_0)-E^{(tot)}(Z)}},\quad T_2=2\sqrt{2m_p}\int_{cA_0}^{A_0}\frac{dZ}{\sqrt{E^{(tot)}(A_0)-E^{(tot)}(Z)}},\quad c=0.99 \tag{9}$$

To remove the singularity from T_2, one can write

$$E^{(tot)}(A_0)-E^{(tot)}(Z)=(A_0-Z)H^{(tot)}(A_0,Z),H^{(tot)}(A_0,Z)\Big|_{Z=A_0}\neq 0 \tag{10}$$

Similar to $E^{(tot)}(Z)$, $H^{(tot)}(A_0,Z)$ can be written in the form defined in Eq. (2) whose components H_{pi} and $H_{ph/pt}$ are defined by

$$H_{pi}=\Gamma_s\sum_{n=1}^{2}\left(\kappa_n\left(\frac{1}{1+\chi_n\zeta_n}-\frac{\left(\zeta_n-\chi_n\right)^2}{3\left(1+\chi_n\zeta_n\right)^3}\right)+\sum_{m=1}^{8}\sum_{k=0}^{m}\nu_{nmk}\left(\frac{\chi_n^{2k}+\zeta_n^{2k}-\sum_{p=1}^{2k+1}\chi_n^{2k-p+1}\zeta_n^{p-1}}{\left(1+\zeta_n^2\right)^m\left(1+\chi_n^2\right)^m}\right)\right) \tag{11}$$

$$H_{ph/pt}=\Gamma_v\sum_{n=1}^{2}\sum_{j=1}^{2}\left(\kappa_{nj}\left(\frac{1}{1+\chi_{nj}\zeta_{nj}}-\frac{\left(\zeta_{nj}-\chi_{nj}\right)^2}{3\left(1+\chi_{nj}\zeta_{nj}\right)^3}\right)+\sum_{m=1}^{7}\sum_{k=0}^{m}\nu_{njmk}\left(\frac{\chi_{nj}^{2k}+\zeta_{nj}^{2k}-\sum_{p=1}^{2k+1}\chi_{nj}^{2k-p+1}\zeta_{nj}^{p-1}}{\left(1+\zeta_{nj}^2\right)^m\left(1+\chi_{nj}^2\right)^m}\right)\right) \tag{12}$$

where $\zeta_n=A_{0_n}\lambda^{-1}$, $\zeta_{nj}=A_{0_n}\lambda_j^{-1}$, $A_{0_1}=A_0+L$, $A_{0_2}=A_0-L$ and the other parameters are as

$$\begin{gathered}\kappa_n=(-1)^{(n+1)}G_1\lambda^{-1},\quad \kappa_{nj}=(-1)^{(n+1)}G_{1j}\lambda_j^{-1}\\ \upsilon_{nmk}=(-1)^{(n+1)}\binom{m}{k}G_{2m-1}\lambda^{-1},\quad \upsilon_{njmk}=(-1)^{(n+1)}\binom{m}{k}G_{(2m-1)j}\lambda_j^{-1}\end{gathered} \tag{13}$$

Substituting Eq. (10) into Eq. (9) and letting $Z=A_0\sin^2\phi$, T_2 is obtained as

$$T_2=4\sqrt{2m_pA_0}\int_{\sin^{-1}\sqrt{c}}^{\pi/2}\frac{\sin\phi}{\sqrt{H^{(tot)}\left(A_0,\phi\right)}}d\phi \tag{14}$$

Note that the oscillation frequency is the reciprocal of amplitude of motion.

4. Numerical results

Based on the proposed formulations, numerical results are presented in this section for the vdW interactions and oscillation frequency of metallic nanoparticle-LPN oscillators. The values of constant parameters required for numerical evaluations are listed in Table 1.

Table 1. Constants required for numerical evaluations [19].

Mean volume density of Ag	0.0587 $Å^{-3}$
Mean volume density of Au	0.0590 $Å^{-3}$
Well depth (Ag-Ag)	0.036 kcal/mol
Well depth (Au-Au)	0.039 kcal/mol
VdW diameter (Ag-Ag)	2.8045 Å
VdW diameter (Au-Au)	2.9337 Å
Well depth (intermediate layer-intermediate layer)	3.4 kJ/mol
Well depth (head group-head group)	5 kJ/mol
Well depth (tail group-tail group)	1.8 kJ/mol
VdW diameter (intermediate layer-intermediate layer)	4.7 Å
VdW diameter (head group-head group)	4.7 Å
VdW diameter (tail group-tail group)	4.7 Å
Mass density of Ag	10.49×10^{-27} kg/$Å^3$
Mass density of Au	19.32×10^{-27} kg/$Å^3$
Length of LPN	300 Å

For silver and gold nanoparticles, the distributions of vdW interaction force and potential energy are depicted in Fig. 2(a) and Fig. 2(b), respectively. This figure shows that the nanoparticle is sucked into the LNT by an attractive interaction force generated near the two ends of the LNT. In other locations, the potential energy remains unchanged and thus the nanoparticle experiences a constant velocity in this range. It can be further observed that the minimum potential energy of silver nanoparticle is greater than that of gold nanoparticle.

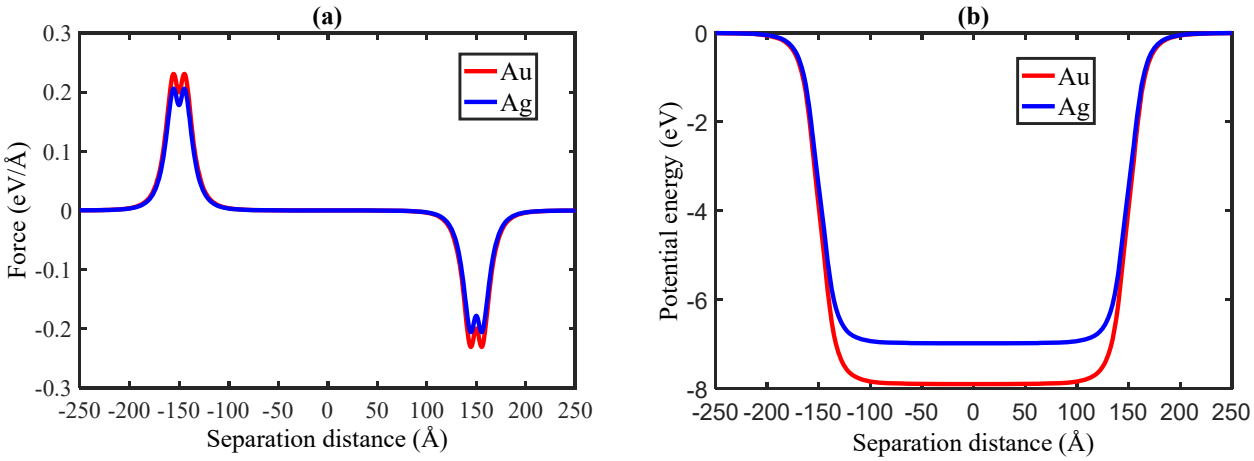

Figure 2. Distribution of (a) interaction force (b) potential energy related to silver and gold nanoparticles $\left(R_p = 50Å, L_h = 8Å, L_t = 15Å\right)$.

Using the Runge-Kutta numerical integration technique, the variations of separation distance and velocity with the time are demonstrated in Fig. 3(a) and Fig. 3(b), respectively. In this figure, the nanoparticle is released at the right end of the LNT with no initial velocity. As shown, the nanoparticle oscillates about its preferred position in the middle of the LNT, where it has the maximum velocity. It can also be noted that the amplitude peak of silver and gold nanoparticles is similar,

whereas the maximum velocity of silver nanoparticle is 14.27 m/s, which is 27.64% greater than that of gold nanoparticle. According to the obtained results, for the identical geometrical parameters and initial conditions, the oscillation frequency of silver nanoparticle is 0.2089 GHz, which is 27.69% higher than that of gold nanoparticle.

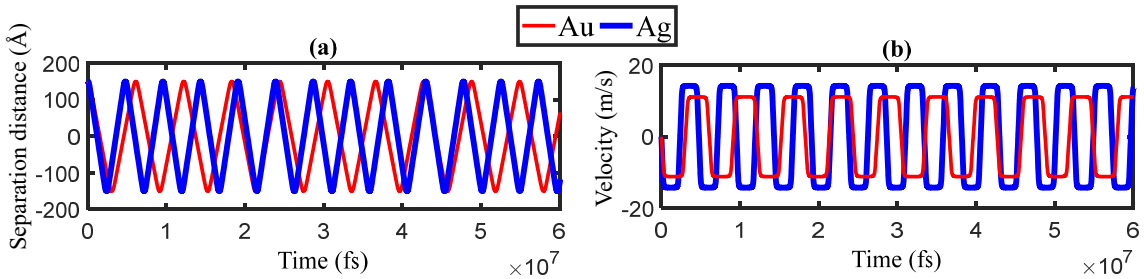

Figure 3. Variation of (a) separation distance (b) velocity with the time for silver and gold nanoparticles $\left(R_p = 50\text{Å}, L_h = 8\text{Å}, L_t = 15\text{Å}\right)$.

For different radii of silver nanoparticle, the variation of frequency with the amplitude is graphically illustrated in Fig. 4(a). In this figure, it is assumed that the nanoparticle is released without an initial velocity from a position where attractive vdW force exists. As illustrated, there is a certain amplitude at which the oscillation frequency peaks. This amplitude and its associated frequency are known as critical amplitude and maximum frequency, respectively. As depicted, the frequency curve ascends and descends for amplitudes smaller and greater than the critical one. Numerical results indicate that increasing the nanoparticle radius causes the critical amplitude to increase, while it causes the maximum frequency to decrease. In order to explore how oscillation frequency varies with the initial velocity, Fig. 4(b) is presented. In this figure, it is supposed that an initial velocity is imparted to the nanoparticle at the preferred position of the system. It is evident form Fig. 4 that nanoparticles of smaller radii generate higher frequencies for a given initial condition. Additionally, the ultimate value of velocity in Fig. 4(b) relates to the escape velocity which decreases as nanoparticle radius gets larger.

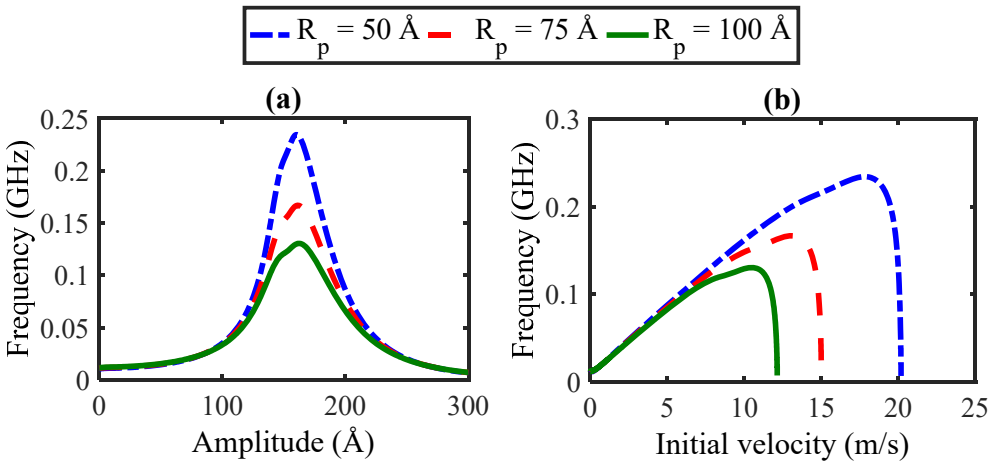

Figure 4. Variation of (a) frequency with the amplitude (b) frequency with the initial velocity related to different radii of silver nanoparticle $\left(L_h = 8\text{Å}, L_t = 15\text{Å}\right)$.

The effects of head group and tail group thicknesses on the variations of frequency with the amplitude and frequency with the initial velocity of silver nanoparticle are examined in Fig. 5(a) and Fig. 5(b), respectively. As shown, the critical amplitude is independent of head group and tail

group thicknesses. Furthermore, compared to head group thickness, the tail group thickness has a minor effect on the oscillatory behavior of the system. Based on the numerical results, 12.5% and 33.33% increases in the head group and tail group thicknesses lead to 6.02% and 1.15% decreases in the values of maximum frequency, respectively.

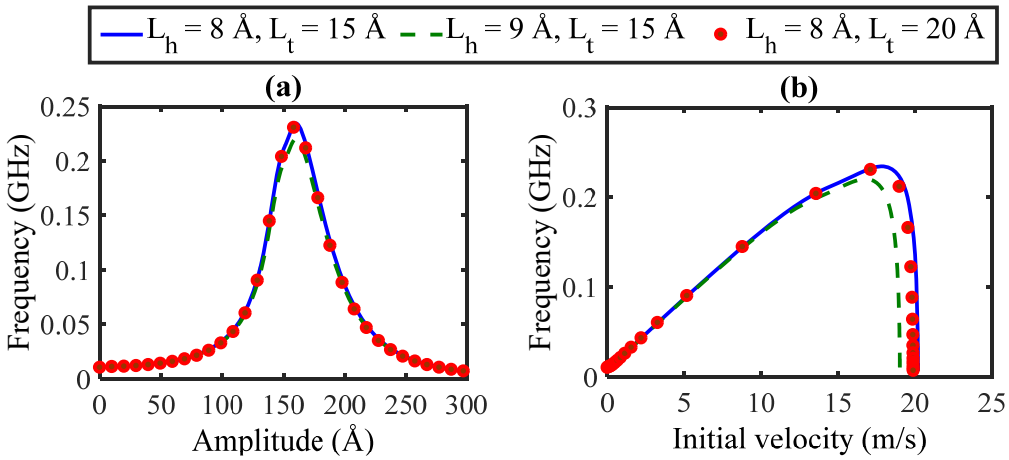

Figure 5. Variation of (a) frequency with the amplitude (b) frequency with the initial velocity of silver nanoparticle related to different thicknesses of head and tail groups $\left(R_p = 50\text{Å}\right)$.

5. Conclusion

In this paper, a continuum-based model was presented to investigate the dynamic behavior of metallic nanoparticle-LNT oscillators. Two types of nanoparticles (silver and gold) were studied and represented as dense spheres. The LNT was assumed to be made up of six layers: two head groups, two middle layers, and two tail groups. Analytical expressions were first derived to determine vdW interactions between the two interacting nanostructures. The equation of motion was solved numerically to obtain the time histories of displacement and velocity of nanoparticles inside LNT. Utilizing the conservation of mechanical energy principle, a semi-analytical frequency statement was also provided into which the effects of geometrical parameters and initial conditions were incorporated. It was discovered that the oscillation frequency associated with silver nanoparticle is higher than that of gold one. It was further demonstrated that an increase in nanoparticle radius results in a decrease in the maximum frequency and an increase in the critical amplitude. Numerical results also indicated that the frequency response is less affected by tail group thickness compared to head group one. Additionally, the critical amplitude was determined to be unaffected by the thickness of the head/tail group, whereas the maximum frequency slightly decreases as the thickness of the head/tail group increases.

REFERENCES

1. Y. Wang, S. Lu, W. He, S. Gong, Y. Zhang, X. Zhao, Y. Fu, Z. Zhu, “Modeling and characterization of the electrical conductivity on metal nanoparticles/carbon nanotube/polymer composites”, *Scientific Reports* **12** (1), 10448 (2022).
2. S. Jafarzadeh, S. M. Jafari, “Impact of metal nanoparticles on the mechanical, barrier, optical and thermal properties of biodegradable food packaging materials”, *Critical Reviews in Food Science and Nutrition* **61** (16), 2640-2658 (2021).
3. A. Naganthran, G. Verasoundarapandian, F. E. Khalid, M. J. Masarudin, A. Zulkharnain, N. M. Nawawi, M. Karim, C. A. Che Abdullah, S. A. Ahmad, “Synthesis, characterization and biomedical application of silver nanoparticles”, *Materials* **15**(2), 427 (2022).

4. Z. Yang, D. Wang, C. Zhang, H. Liu, M. Hao, S. Kan, D. Liu, W. Liu, "The applications of gold nanoparticles in the diagnosis and treatment of gastrointetinal cancer", *Frontiers in Oncology* **11**, 819329 (2022).
5. R. Sakthi Devi, A. Girigoswami, M. Siddharth, K. Girigoswami, "Applications of gold and silver nanoparticles in theranostics", *Applied Biochemistry and Biotechnology* **194**(9), 4187-4219 (2022).
6. G. Lamour, A. Allard, J. Pelta, S. Labdi, M. Lenz, C. Campillo, "Mapping and modeling the nanomechanics of bare and protein-coated lipid nanotubes", *Physical Review X* **10**(1), 011031 (2020).
7. H. Bi, Z. Chen, L. Guo, Y. Zhang, X. Zeng, L. Xu, "Fabrication, modification and application of lipid nanotubes", *Chemistry and Physics of Lipids* **248**, 105242 (2022).
8. I. Gözen, P. Dommersnes, "Biological lipid nanotubes and their potential role in evolution", *The European Physical Journal Special Topics* **229**(17), 2843-2862 (2020).
9. J. F. Nagle, S. Tristram-Nagle, "Structure of lipid bilayers", *Biochimica et Biophysica Acta (BBA)-Reviews on Biomembranes* **1469**(3), 159-195 (2000).
10. W. Rawicz, K. C. Olbrich, T. McIntosh, D. Needham, E. Evans, "Effect of chain length and unsaturation on elasticity of lipid bilayers", *Biophysical Journal* **79**(1), 328-39 (2000).
11. H. Träuble, D. H. Haynes, "The volume change in lipid bilayer lamellae at the crystalline-liquid crystalline phase transition", *Chemistry and Physics of Lipids* **7**(4), 324-335 (1971).
12. O. Berger, O. Edholm, F. Jähnig, "Molecular dynamics simulations of a fluid bilayer of dipalmitoylphosphatidylcholine at full hydration, constant pressure, and constant temperature", *Biophysical Journal* **72**(5), 2002-2013 (1997).
13. R. Qiao, A. P. Roberts, A. S. Mount, S. J. Klaine, P. C. Ke, "Translocation of C_{60} and its derivatives across a lipid bilayer", *Nano Letters* **7**(3), 614-619 (2007).
14. H. Wang, S. Michielssens, S. L. Moors, A. Ceulemans, "Molecular dynamics study of dipalmitoylphosphatidylcholine lipid layer self-assembly onto a single-walled carbon nanotube", *Nano Research* **2**, 945-954 (2009).
15. S. J. Marrink, H. J. Risselada, S. Yefimov, D. P. Tieleman, A. H. De Vries, "The MARTINI force field: coarse grained model for biomolecular simulations", *The Journal of Physical Chemistry B* **111**(27), 7812-7824 (2007).
16. J. C. Shelley, M. Y. Shelley, R. C. Reeder, S. Bandyopadhyay, P. B. Moore, M. L. Klein, "Simulations of phospholipids using a coarse grain model", *The Journal of Physical Chemistry B* **105**(40), 9785-9792 (2001).
17. D. Baowan, B. J. Cox, J. M. Hill, "Instability of C_{60} fullerene interacting with lipid bilayer", *Journal of Molecular Modeling* **18**, 549-557 (2012).
18. W. Sukchom, K. Chayantrakom, P. Satiracoo, D. Baowan, "Penetration of carbon nanocylinder through a lipid bilayer", *Southeast Asian Journal of Sciences* **2**(1), 87-100 (2013).
19. F. Sadeghi, R. Ansari, M. Darvizeh, "Mechanics of metallic nanoparticles inside lipid nanotubes: suction and acceptance energies", *Proceedings of the Institution of Mechanical Engineers, Part C: Journal of Mechanical Engineering Science* **231**(13), 2540-2553 (2017).
20. W. Al Misba, H. S. Mavikumbure, M. M. Rajib, D. L. Marino, V. Cobilean, M. Manic, J. Atulasimha, "Spintronic physical reservoir for autonomous prediction and long-term household energy load forecasting", *IEEE Access* **11**, 124725 (2023).
21. S. Wittrock, S. Perna, R. Lebrun, K. Ho, R. Dutra, R. Ferreira, P. Bortolotti, C. Serpico, V. Cros, "Non-hermiticity in spintronics: oscillation death in coupled spintronic nano-oscillators through emerging exceptional points", *Nature Communications* **15**(1), 971 (2024).
22. N. Leroux, A. De Riz, D. Sanz-Hernández, D. Marković, A. Mizrahi, J. Grollier, "Convolutional neural networks with radio-frequency spintronic nano-devices", *Neuromorphic Computing and Engineering* **2**(3), 034002 (2022).
23. Q. Zheng, J. Z. Liu, Q. Jiang, "Excess van der Waals interaction energy of a multiwalled carbon nanotube with an extruded core and the induced core oscillation", *Physical review B***65**(24), 245409 (2002).